Final Report

IR DETECTORS TECHNOLOGY

Project:

SPC-004064

July 2001

Issuing Organization and Point of Contact
Institute of Physics, Charles University

Prof. Pavel Höschl

Ke Karlovu 5
CZ-121 16 Prague 2
Czech Republic
FAX (+420 2) 24922797

REPORT DOCUMENTATION PAGE

Form Approved OMB No. 0704-0188

1. REPORT DATE *(DD-MM-YYYY)*	2. REPORT TYPE	3. DATES COVERED *(From – To)*
31-07-2001	Final Report	10 August 2000 - 07-Sep-01

4. TITLE AND SUBTITLE

INFRARED TECHNOLOGY DETECTORS

5a. CONTRACT NUMBER
F61775-00-WE064

5b. GRANT NUMBER

5c. PROGRAM ELEMENT NUMBER

6. AUTHOR(S)

Professor Pavel Hoschl

5d. PROJECT NUMBER

5d. TASK NUMBER

5e. WORK UNIT NUMBER

7. PERFORMING ORGANIZATION NAME(S) AND ADDRESS(ES)

Charles University
Institute of Physics
PRAGUE 2 CZ-121 16
Czech Republic

8. PERFORMING ORGANIZATION REPORT NUMBER

N/A

9. SPONSORING/MONITORING AGENCY NAME(S) AND ADDRESS(ES)

EOARD
PSC 802 BOX 14
FPO 09499-0014

10. SPONSOR/MONITOR'S ACRONYM(S)

11. SPONSOR/MONITOR'S REPORT NUMBER(S)
SPC 00-4064

12. DISTRIBUTION/AVAILABILITY STATEMENT

Approved for public release; distribution is unlimited.

13. SUPPLEMENTARY NOTES

14. ABSTRACT

This report results from a contract tasking Charles University as follows: The contractor will perform a series of in-situ Hall effect and conductivity measurement of CdTe/CdZnTe material to determine dependence of temperature above the melting point. A new setup for high temperature galvanomagnetic measurements enabling better control of the Cd overpressure above the melt will be constructed. Based on the experimental and theoretical results a model will be determined and defect concentrations in samples annealed under defined conditions will be further verified. Near perfect (CdZn)Te crystals of diameter up to 10 cm under a defined Cd overpressure will be prepared and evaluated.

15. SUBJECT TERMS
EOARD, Sensor Technology, Detector Technology

16. SECURITY CLASSIFICATION OF:			17. LIMITATION OF ABSTRACT	18, NUMBER OF PAGES	19a. NAME OF RESPONSIBLE PERSON
a. REPORT	b. ABSTRACT	c. THIS PAGE			David M. Burns, Lt Col, USAF
UNCLAS	UNCLAS	UNCLAS	UL	49	19b. TELEPHONE NUMBER *(Include area code)* +44 (0)20 7514 4955

Standard Form 298 (Rev. 8/98)
Prescribed by ANSI Std. Z39-18

Distribution:

Dr. Meimei Tidrow, BMDO	1 copy
Dr. Richard Hu, BMDO	1 copy
Lt.Col.R.Burns, EOARD	1 copy

I. INTRODUCTION

This final report contains the results of the project SPC-004064 and concentrates mainly latest results of measurement of electrical conductivity in liquid CdTe and under a defined Cd overpressure. Attention is also paid to evaluation of high temperature galvanomagnetic measurements in order to find optimal cooling conditions for fabrication of near-stoichiometric single crystals from the point of view of chemical self-diffusion of Cd. Due to the fact, that interest in fabrication of large, homogeneous high-resistivity CdTe and (CdZn)Te for gamma ray detectors applications strongly increases, conditions for preparation of such a material with a minimized total concentrations of defects and thus with improved detection properties are looked for. A possibility to use measurements of optical absorption to evaluate concentrations of shallow absorption levels are discussed as well. The topics, which were in detail described in the Progress report to this project are not repeated in the Final report.

II. HIGH TEMPERATURE ELECTRICAL PROPERTIES OF LIQUID CDTE

A. Introduction

CdTe and (CdZn)Te with a small Zn content have considerable application in optoelectronics devices. These materials are used as substrates for epitaxial growth of HgCdTe layers for infrared detectors, for a fabrication of gamma ray detectors and electrooptical modulators. All these applications require large bulk single crystals with defined electrical and optical properties.

The growth of single crystals from the melt represents the dominating method of preparation of crystals to the above mentioned purposes. The most commonly used experimental arrangement is the vertical directional cooling of the stoichiometric melt. The routine fabrication of CdTe and (CdZn)Te crystals with pre-defined electrical and optical parameters has not been fully managed. This fact is caused mainly by relatively non-standard physicochemical properties, such as a high partial pressure of a more volatile component around

the melting point, conservation of bonds between Cd and Te atoms in liquid CdTe and a low thermal conductivity, which substantially differs in the liquid and in the solid state. Especially the first two properties influence the growth of single crystals from the melt and therefore we will discuss them in the next chapter more deeply. The bad thermal conductivity of the solid results only in a gradual slowdown of the crystal growth, especially in the last stage, when the heat outlet of the latent heat of crystallization is weak.

Therefore a method is looked for, how to receive maximum information about the whole process of preparation of single crystals from the melt and especially about the way, how the growth and quality of single crystals is influenced by external growth conditions in order to optimize the process. So far very little is known about the state of the melt before the beginning of crystallization and about the respective process of solidification of the melt. Therefore we concentrated our effort on these two topics.

It came out, that the measurement of electrical conductivity is suitable for these purposes. Originally we wanted to study also the Hall effect, which in general comprises more information about the current carriers, but due to the fact, that this effect is orders of magnitude smaller than the conductivity, it is strongly influenced by the noise, which dominates the signal at temperatures above 1000°C.

B. The properties of liquid CdTe and preparation of crystals from the melt

The process of crystal growth from the melt can be divided in three stages.

1st stage - the melt

Two phases coexist - the gas phase (G) and the liquid phase (L), when the state of the melt is defined by temperature T and a pressure of one of the components e.g. Cd (P_{Cd}). The congruent melting point of CdTe is T_m=1092°C. Relatively little is known about the properties of liquid CdTe. To describe the liquid a Jordan's model of regular associated solutions is applied. Model calculations yield, that the stoichiometric liquid is only partially dissociated (about 5 percent) into Cd and Te atoms [1]. The conservation of bonds in

liquid CdTe was confirmed by neutron diffraction experiments [2], Hall effect [3], electrical conductivity [3–6]. Also theoretical calculations [7] suppose existence of Te chains, to which Cd is bonded. Muhlberg [8] found out during the growth, that a better quality single crystals can be obtained from highly superheated melts, when the dissociation of the liquid is higher. Most experimental measurements were so far performed only in dependence of temperature, without a concrete knowledge of a partial pressure of one of the components. That is why the experimental dependences obtained such a way must be viewed with a great care. As will be shown later in the report, the dependence on the partial pressure of one of the components is strong.

2nd stage - the solidification

This stage is characterized by coexistence of three phases - the gas(G), the liquid (L) and the solid (S). The state of both the liquid and solid phases is defined by the partial pressure of one of the components on the three phase line. We found out [9], that the Cd pressure corresponding to the stoichiometric solid is P_{Cd}=1.9atm and to the stoichiometric liquid P_{Cd}=1.2atm. It means, that stoichiometric solid is fabricated by solidification of the Cd rich liquid, while solidification of stoichiometric liquid results in Te rich solid. The dominating component in the vapor phase is in both cases Cd.

Another interesting point on the three phase line is the point, at which the gas phase is stoichiometric, it means when congruent sublimation occurs. This pressure is approx P_{Cd}=0.12atm. At this pressure at the given temperature is the total pressure above the completely solidified liquid minimal and the material sublimes strongly. Our experiments have shown, that e.g. electrical conductivity can be measured only at pressures P_{Cd} >1.1 atm, when sublimation does not influence the performed measurements.

3rd stage - the solid

Two phase coexist during the cooling of the solid - the gas (G) and the solid (S). The state of the solid is in this case determined by temperature and a pressure of one of the components, e.g. Cd. We studied the processes occurring within the range of coexistence of S and L within the last years. We found out to evaluate from annealing experiments and from

in situ [9–11] galvanomagnetic measurements, when we measured electrical conductivity and Hall effect the following conclusions

a) to determine the line $P_{Cd(S)}$ in the P-T diagram, which corresponds to the stoichiometric solid, it means the mode suitable for cooling of the crystal to keep its stoichiometry

b) to clarify the processes of diffusion which define the process of establishing of the equilibrium in the crystal, it means an optimized time procedure of crystal cooling.

It is clear, that information about the equilibrium of the liquid and gas phases are insufficient. No authors studied both the temperature and the pressure dependence of any parameter, which could provide information about cooling of the liquid including the phase transition between the solid and the liquid. We tried to study the electrical conductivity in dependence of T and P_{Cd} in the melt and during the solidification of the melt.

C. Experimental setup

One of the main goals of the present project is to measure galvanomagnetic properties in liquid CdTe and CdZnTe under a defined Cd overpressure. To complete this difficult task we constructed a new experimental setup based on establishing a well defined partial pressure of the volatile component in a semi-open system originally described by Van Doorn [12], which he used in the Philips laboratories. The principle of the method is apparent from Fig. 1, the total arrangement of the experiment from Fig. 2.

The CdTe sample is located in the plateau of constant temperature. The pressure of Cd vapor is kept by evaporation of Cd from the source. Cd condenses on the wall at the place, where the temperature reaches the boiling point of Cd. The liquid Cd then flows along the wall to places with a higher temperature where it again evaporates. This cycle is similar to the way, how the diffusion pump works. The place of Cd condensation depends on the pressure of Ar, which is in equilibrium with the Cd pressure. The pressure of Ar is kept on a constant value with a pressure gauge, which enables an automatic control of pressure with a high precision up to 1.6 atm. The detailed arrangement of the measuring cell is apparent

from Fig. 3.

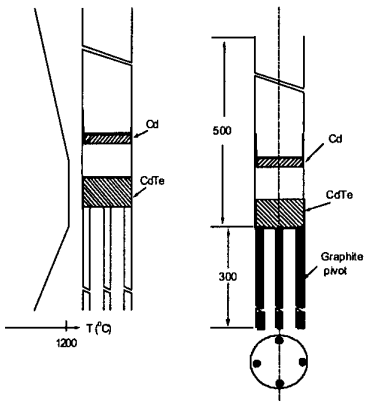

FIG. 1. The scheme of the measuring cell within the Van Doorn adjustment.

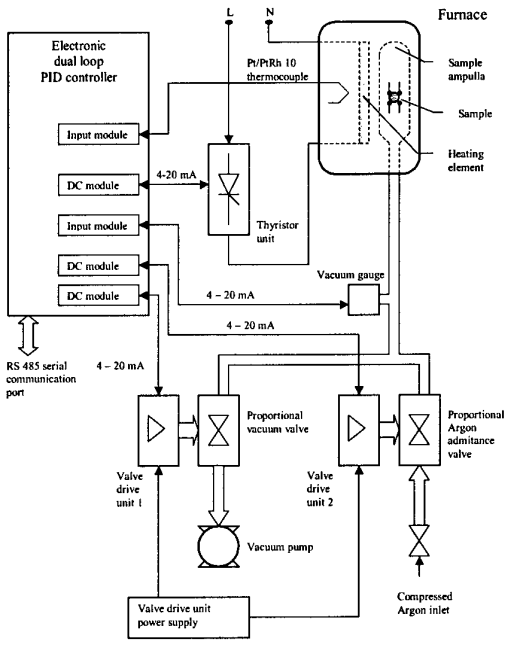

FIG. 2. Schematic drawing of the furnace control. Both temperature and pressure are controlled by Eurotherm 2704 dual loop, high accuracy and stability process controller.

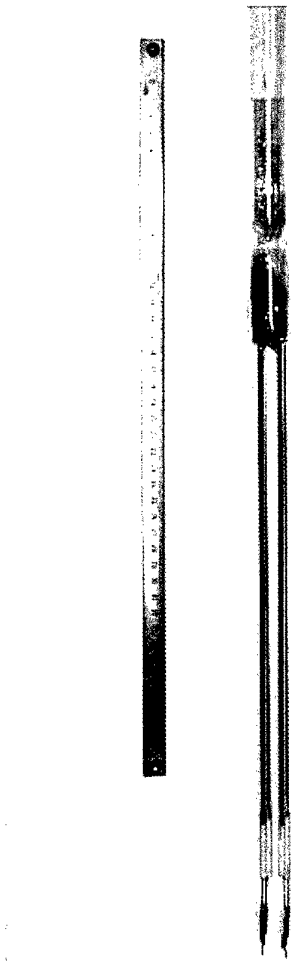

FIG. 3. The measuring ampoule for the measurements of conductivity of liquid and solid CdTe and (CdZn)Te in the Van der Pauw configuration. Four graphite contacts are seen beneath, the sample is at tho bottom of the ampoule. The Cd source is above the bottleneck.

The measurements were performed in both the DC and the AC modes, when better results were obtained in the DC mode. We concentrated on measurements of the electrical conductivity, because the measurements of the Hall coefficient were affected by a great experimental error. Furthermore the measured dependences showed a similar slopes and trends as the data from the measurements of electrical conductivity. It comes out, that

should it be necessary to study the Hall effect in the liquid CdTe, a new type of the measuring cell, which enables to measure very thin layers will have to be constructed. Preliminarily we start to work on this topic.

D. Electrical conductivity of liquid CdTe

The dependence of electrical conductivity in dependence of temperature and Cd partial pressure is shown on Fig. 4. A fully new result is the dependence of the degree of supercooling of the melt on Cd partial pressure. This result, which is apparent from the figure, is to some extent unexpected. The supercooling ΔT decreases, when P_{Cd} increases. For P_{Cd}=1.3, 1.4, and 1.6 atm, ΔT=8, 13, 23°C, respectively. The cooling/heating rate 15°C/hour was used in the measurement. We can compare our results with [13], where the dependence of supercooling on Te mole fraction in Te-rich CdTe x is reported. For the decreasing x=0.55, 0.51, 0.5 the supercoling decreases: ΔT=100, 75, 38°C, respectively. We can conclude, that both in Te-rich and in Cd-rich material ΔT decreases, when the content of Cd in CdTe increases. This fact has an impact to the crystal growth because the large-diameter single crystals can be grown only in the regime of minimized supercooling. This condition is better fulfilled in the Cd-rich material, than in the stoichiometric one. The crystal growth at high pressure of Cd should be thus examined to verify such a possibility. In case of stoichiometric material the supercooling must be minimized decreasing the cooling rate or by a proper arrangement of the crystal growth apparatus.

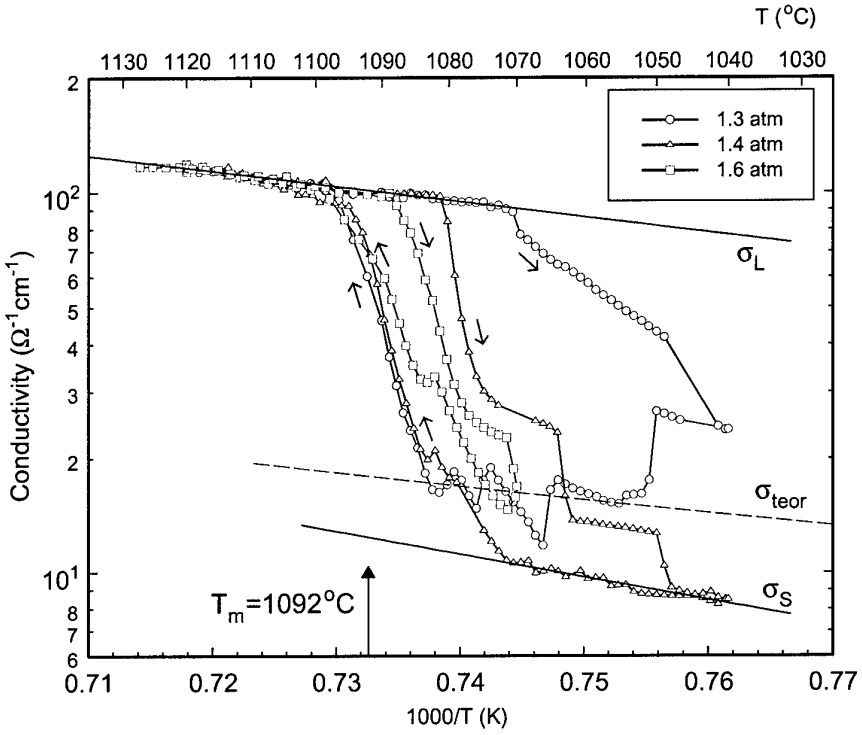

FIG. 4. The conductivity of solid and liquid CdTe vs temperature at various Cd pressures P_{Cd} =1.3, 1.4, 1.5 atm. The direction of the cooling/heating loop is indicated by arrows. σ_L and σ_S show fit of σ in the liquid and solid, σ_{teor} is theoretical conductivity of solid. The melting point T_m is labelled as well.

The guide full lines in Fig. 4 describe σ of solid and liquid. In case of σ_S in the solid, which is defined by

$$\sigma_S = 3.3 \times 10^5 \exp(-1.2\text{eV}/k_bT)\ (\Omega^{-1}\text{cm}^{-1}), \tag{1}$$

the interpretation is not clear. The comparable theoretical curve σ_{teor} calculated within our model is higher and its slope is less, only 0.8 eV. The conductivity in the liquid

$$\sigma_L = 9.1 \times 10^4 \exp(-0.8\text{eV}/k_bT)\ (\Omega^{-1}\text{cm}^{-1}) \tag{2}$$

agrees well with [6], where the slope 0.85 eV was reported. The σ_L can be properly ap-

proximated within our model of native defects in the solid [3], if we set deep donor level with density $\sim 10^{22}$ cm^{-3} about 1 eV below the bottom of the conduction band. On such a level Te antisite Te_{Cd} is often assumed. Concluding from that, the liquid CdTe behaves electrically as semiconductor with high density of deep defects, mostly donors. These defects are probably dissociated free Te or Cd atoms. Their energy levels are deep below the Fermi level, which results about 200 meV below the conduction band. The transport properties are dominated by electrons in conduction band excited from the donors. Increasing temperature, the fraction of dissociated species increases and the material is expected to become a metal - second order phase transition. Looking for such a crossing point (semiconductor-semimetal) is desirable to understand the statistics of the defects and transport mechanisms in the liquid.

A comparison of our experiment with other relevant data is presented in Fig. 5. In case of [4] and [5] the measurements without defined P_{Cd} were done. These curves have similar features as our σ measured at the cooling at 1.3 atm. As we have observed, the sublimation of the material is high at this pressure and the phase transition is difficult to be proven. Much better results are published in [6], which presents σ_S at P_{Cd}=1.42 atm very close to our theoretical value and phase transition including supercooling well pronounced. The melting point is about 10°C below correct value. Indirect method to measure electrical conductivity in closed system by multifrequency eddy current sensor is reported in [14]. This method looks optimum for the examination of the phase transition and to collect the essential data for the crystal growth. The absolute value of σ is affected by a systematic error and σ is less than data from direct measurements.

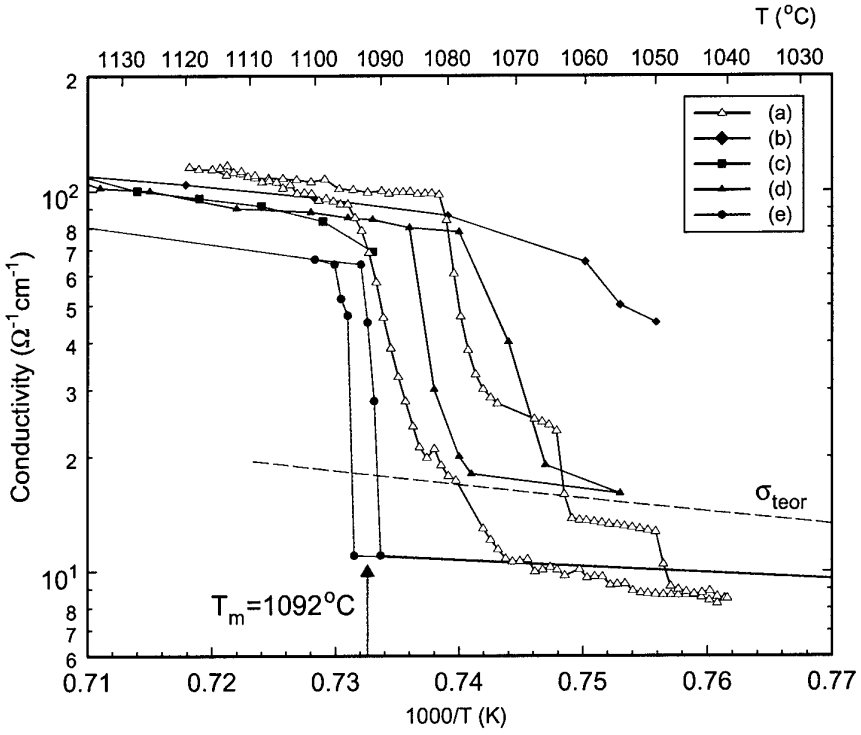

FIG. 5. Comparison of our measurement of σ at 1.4 atm (a) with data reported by other workers. (b) [4], (c) [5], (d) [6], (e) [14]

E. Future plans

The reproducible growth of high-quality single crystals requires a detailed understanding of the relationships between the controllable growth parameters and the properties of CdTe, (CdZn)Te, especially in solid and liquid near three phase line in P-T diagram and phase equilibria during the crystal growth. High temperature *in-situ* electrical measurements at defined thermodynamic conditions are an effective tool to obtain relevant data from this field. Based on the results discussed above we plan the following experiments:

1. To measure electrical conductivity of liquid CdTe at high Cd pressures (P_{Cd}=1.6 - 10 atm). The maximum P_{Cd} at the three phase line in the phase diagram will be looked for

and its neighborhood studied in detail. The properties of liquid and solid near this critical point will be evaluated.

2. To study the influence of the overheating and of the cooling velocity to the supercooling of the melt and to propose an optimum overheating for the crystal growth.

3. To study in the liquid CdTe the point, where the semiconducting behaviour changes to the semimetallic one. To complete the P-T phase diagram by the line at which this phase transition of second order occurs.

4. There is an open question about the dependence of the growth direction, in our crystals of type (111), which changes to the direction (100), if P_{Cd} is increased. We would like to prove and explain such observation and to specify the limiting P_{Cd}, which determines such conversion.

III. CHEMICAL SELF-DIFFUSION IN CDTE

A. Introduction

The chemical diffusion coefficient D is a key parameter characterizing an annealing time, which is necessary to attain the thermodynamic equilibrium at given temperature or to produce a desired gradient in composition. Chemical self-diffusion experiments in near stoichiometric bulk CdTe are carried by *in-situ* high temperature electrical measurements, where the response time of the free carrier concentration or electrical conductivity corresponding to step changes of ambient partial Cd pressure (P_{Cd}) are measured, for a review, see [15]. The only relevant experimental data on undoped samples are found in [6], which reports on the diffusion at temperatures T=700–900^{0}C and in [16] for T=600–800^{0}C.

The aim of this paper is to check the above mentioned data and to repeat the measurements in CdTe of a better purity than they were performed before. No experimental measurements have been made since $\sim$ 1980 and new experiments are highly desirable in this field.

B. Experiment

Undoped CdTe single crystals were produced by the Vertical Gradient Freeze method [17] at Cd overpressure 1-1.3 atm. 6N purity starting elements were used in all growth runs. *In situ* galvanomagnetic measurements of conductivity σ and Hall effect by the Van der Pauw method on samples with dimensions 10x10x1.5 mm^3 were performed in two zone furnace at temperatures up to 1050°C and P_{Cd} controlled by a temperature T_{Cd} of the cold zone [3].

Time evolution of samples after step-like change of P_{Cd} in the interval of P_{Cd} one order of magnitude below and above the ideal stoichiometry line was measured and the chemical diffusion coefficient of cadmium telluride D was determined as a function of temperature in the temperature range T=500–700°C. The delay of the furnace to reach stable state after the step-like change of T_{Cd} was about 10 min.

C. Theory

The analysis of high temperature measurements allowed us to establish the region in the pressure-temperature (P-T) phase diagram to obtain intrinsic CdTe and to correlate them with the stoichiometry of the samples. The position of the theoretical stoichiometry line (the so called p-n line) in the form

$$P^S = 8 \times 10^5 \exp(-1.76 \times 10^4/T) \text{ (atm)}. \quad (3)$$

was found [9]. Simultaneously, the galvanomagnetic properties of CdTe were used to establish formation energies and entropy terms, which determine the properties of native point defects [3].

Deviating from P^S, native point defects which represent excess or deficit of Cd are created and diffuse in the sample. The favorite electrically active native defects, which dominate in near stoichiometric samples CdTe are Cd interstitial (Cd_I, divalent donor) and Cd vacancy (V_{Cd}, divalent acceptor) [3,18]. In view of the fact, that maximum dissolvable excess of

Cd or Te in solid CdTe is about four times larger than the defect density obtained from electrical measurements [18], neutral native defects are also present in the sample. Their concentration depends much strongly on P_{Cd} than it is in case of charged native defects and they prevail in CdTe in the regions of P-T diagram near the three-phase-line [9]. Charged and neutral defects should be taken into account to describe the chemical diffusion in CdTe properly. They can act both actively transferring material within the sample and passively as traps for the fast moving defects.

Such a complicated structure of native defects results in a necessity to assume $D(\Delta)$ as a function of the stoichiometry deviation Δ. The experimental data show, however, that $D(\Delta)$ is practically independent of Δ in samples near stoichiometry [6,16]. Also in our measurements we were not able to prove any dependence on Δ and we follow the previous approaches.

In our arrangement of a flat sample, the one-dimensional diffusion can be assumed and the diffusion profile of the stoichiometry variations reads

$$\Delta(x,t) = (\Delta_1 - \Delta_0)\Sigma_{n=0}^{\infty}(-1)^n \left[\mathrm{erfc}\left(\frac{nL+x}{2\sqrt{Dt}}\right) + \mathrm{erfc}\left(\frac{(n+1)L-x}{2\sqrt{Dt}}\right)\right] + \Delta_0, \qquad (4)$$

where the initial and final stoichiometry deviations Δ_0, Δ_1, respectively, are calculated within our model [3]. They correspond to Δ of the sample in equilibrium at P_{Cd} before and after the step-like change. L is the thickness of the sample ($0 < x < L$), homogeneous sample is assumed at $t = 0$.

Near P^S, where the divalent electrically active native defects dominate, the defect statistics according to [3,9] is used and profiles of free carrier densities [electrons $n(x,t)$, holes $h(x,t)$] are calculated via their relation to $\Delta(x,t)$. Consequently, the conductivity $\sigma(t)$ is given as

$$\sigma(t) = \frac{e}{L}\int_0^L [\mu_e n(x,t) + \mu_h h(x,t)]dx, \qquad (5)$$

where $\mu_e(T)$, $\mu_h(T)$ are bulk experimental electron and hole mobilities, respectively. The diffusion coefficient D is the only optimized parameter to fit $\sigma(t)$ to the experimental conductivity data.

Below 600°C the surface conductivity manifests in the initial fast relaxation of σ. This effect must be separated to distinguish the bulk diffusion properly.

D. Results and discussion

The chemical self-diffusion was studied at temperatures 500°C, 600°C, and 700°C. The results are summarized in Table I, where the relevant data of other authors are included. The relatively thin samples (1.5 mm) used in our measurements allowed to measure the diffusion at 500°C, where no data were reported yet. On the contrary, fast diffusion at $T \gtrsim 700$°C, which resulted in the response time comparable with the characteristic time of the furnace (10 min), did not allow to establish D definitely. The average chemical diffusion coefficient deduced from data at 500 and 600°C comes out

$$D = 5 \exp(-1.12 \text{ eV}/k_B T). \tag{6}$$

Extrapolating to higher T, our D results higher than that in [16] and is slightly less than in [6]. All the data, however, agree well within estimated experimental uncertainty.

An example of a typical response of the conductivity to the step change of P_{Cd} together with theoretical curves according to (5) is shown in Fig. 6. The logarithm of normalized conductivity is plotted there according to [16] due to its useful linear shape, which is conveniently used in the analysis.

TABLE I. The chemical self-diffusion coefficient. Our results are compared with data published on pure samples in [6,16]. Data with star were extrapolated.

T (°C)	D (cm^2/s)	D (cm^2/s) [6]	D (cm^2/s) [16]
500	$(2.5\pm0.8) \times 10^{-7}$	$*4 \times 10^{-7}$	$*1.3 \times 10^{-7}$
600	$(1.7\pm0.5) \times 10^{-6}$	$*2.5 \times 10^{-6}$	10^{-6}
700	$> 4 \times 10^{-6}$, $*8 \times 10^{-6}$	9×10^{-6}	5×10^{-6}
800	$*2.5 \times 10^{-5}$	2.5×10^{-5}	1.4×10^{-5}
900	$*7.5 \times 10^{-5}$	7×10^{-5}	$*4 \times 10^{-5}$

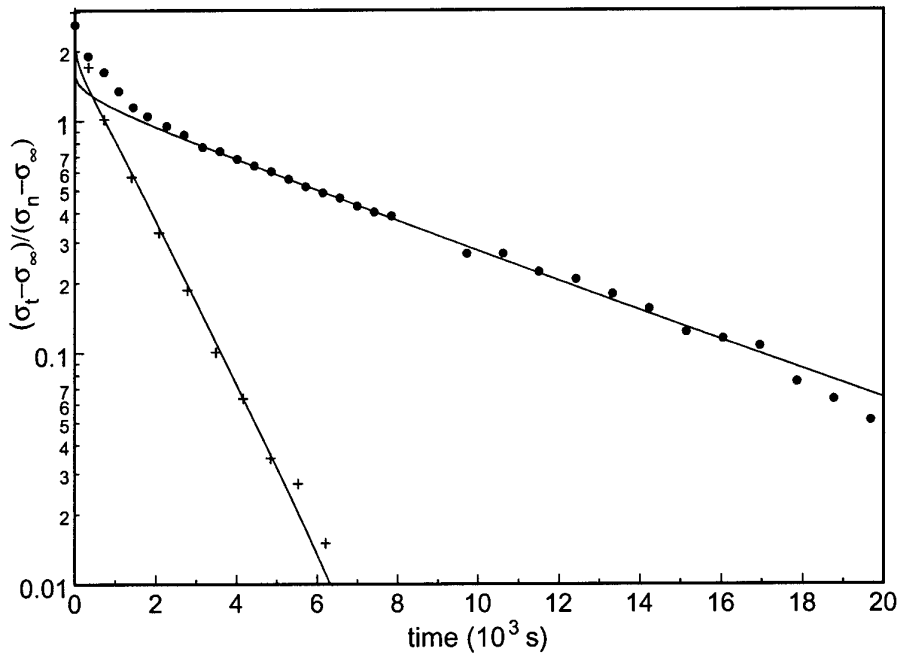

FIG. 6. The logarithm of the normalized conductivity at 500°C (circle) and 600°C (cross) together with theoretical fit (full lines) as a function of time for step-like change in P_{Cd}. The σ_∞ is the conductivity in an infinite time, σ_n is a normalization constant, which attributes unity to a time, from which the curve can be approximated by the exponential decay. The deviations at short time are due to the surface conduction.

The short-time deviations of the experiment from the theory is due to the surface conduction, which starts to prevail at low temperatures above resistive bulk. This effect could be disclosed already in [16], where the data at 600°C are shown. There an incorrect interpretation assuming that the effect is a characteristic for the solution of diffusion equation is suggested. As we see in Fig. 6, the theoretical curve does not fit such strong deviation. Preliminary study shows, that surface conduction depends on P_{Cd} in a similar form as it is in the bulk. The effect of surface conduction in medium temperatures has never been reported before. It complicates the analysis of experimental data in the temperature interval

400-600°C, which is expected to be optimum for a fabrication of low doped high resistive CdTe. Due to this fact the surface conduction should be extensively studied in the future.

Contrary to the report in [6] our diffusion data in increased/decreased P_{Cd} produce very similar D. This finding agrees with the opinion [15], that this effect is due to the capturing of diffusing species on doping impurities. In our pure samples the interaction with impurities can be neglected.

In spite of experimental divergences in various runs, we did not prove any dependence of D on the stoichiometry deviation Δ. It implies that the diffusion coefficients of dominant point defects representing excess or deficit of Cd in the material are close together. This task remains open for future research in which the experimental precision of the conductivity measurements should be improved and the interval of P_{Cd} far from P^S should be chosen.

The parallel investigation of the Hall mobility showed that the variations of transport properties are mostly operated by free electrons and except the lowest $P_{Cd} < 0.1P^S$ the heavy hole transport can be neglected.

E. Conclusion

The coefficient of chemical self-diffusion was established by *in-situ* conductivity measurements. The data agree well with previous results on pure samples. The influence of surface conduction to the electronic properties below 600°C and its dependence on P_{Cd} was found. This effect forces an extended research in this field because of its influence to the fabrication of low doping high resistive CdTe.

IV. CONDITIONS FOR FABRICATION OF HIGH-RESISTIVITY CDTE

A. Introduction

The dominant approach for a production of high resistivity (HR) detector-grade material has been the growth of Cl doped CdTe from Te-rich solutions mainly by the THM method.

Within the last decade substantial effort has been devoted to the growth of high resisitivity (CdZn)Te by the high pressure Bridgman method (HPBM). Here in some cases very high resistivity (10^{11} Ωcm) was achieved. Although HPBM produces large (CdZn)Te ingots, their homogeneity remains an unsolved problem [19]. The manufacture of large homogeneous ingots has not reached a proven stage yet. Continuing effort is still underway to improve the characteristics of CdTe, (CdZn)Te materials in order to achieve reproducible detectors.

One of the key problems limiting further progress in growth of large, perfect, uniform and pure crystals with detector-grade properties is the insufficient understanding of compensation mechanisms leading to the high-resistivity (HR) CdTe, (CdZn)Te. The demands on detector-grade material are comprised in a low dark current and a high mobility-lifetime product of current carriers. To prepare such a material, the concentration of free carriers must be decreased by a proper compensation of shallow levels in the energy gap. CdTe is normally synthesized from 7N purity elements, which implies a level $\sim 10^{16}$ cm^{-3} of foreign impurities. Furthermore, relatively large concentrations of native point defects generated during the crystal growth can be frozen in due to the fact that the diffusion effectively stops at temperature 500°C or even higher depending on the crystal volume. To achieve HR in this case, the equilibrium of concentrations of acceptors and donors $N_A \doteq N_D$ with allowed deviation less than 10^7 cm^{-3} is required, which is difficult to be reached with the state-of-the-art technological procedures. Therefore also attempts to prepare reproducibly HR undoped CdTe controlling the Cd pressure during the growth and minimizing this way deviations from stoichiometric CdTe by vertical and horizontal Bridgman methods were so far not successfull [20].

Clearly, the pinning of the Fermi level to some deep level near the middle of the bandgap is useful to achieve the high resistivity CdTe. This goal is reached by doping with impurities having energy levels near the midgap (e.g. V, Ti) or forming complexes with native defects at the midgap levels. Here, however, the resisitivity is obtained with high concentration of defects leading to the carrier trapping and recombination and therefore poor detector properties of such samples [21].

The purpose of the present paper is to demonstrate the principal difficulties connected with the fabrication of HR material in stoichiometric undoped CdTe or shallow defect doped CdTe. We shall show, how the deep defect doping simplifies this task and suggest a technological procedure to prepare high-resistivity CdTe with minimized unavoidable deep defect doping. Vanadium will be used as a model doping element for demonstration.

B. Experiment

Undoped CdTe single crystals with a diameter up to 100 mm were produced by the Vertical Gradient Freeze method [17] at Cd overpressure 1-1.3 atm. 6N purity starting elements were used in all growth runs. The cooling speed during the crystallization process at temperatures 1120-1080°C was 0.5°C/hour. All crystals were very good quality single crystals filling about 90% of the crucible volume with no macroscopical defects (grain boundaries, twins).

In situ galvanomagnetic measurements of Hall effect by Van der Pauw method on solid samples with dimensions 10x10x1.5 mm^3 at defined Cd pressure P_{Cd} and temperatures up to 1050°C were performed [3]. The theoretical analysis of such measurements allowed us to establish the high temperature intrinsic conditions in the P-T diagram and to correlate them with the stoichiometry of the samples.

C. Theory

The obtaining of high-quality CdTe and (CdZn)Te samples for X- and gamma ray radiation detectors is connected with the demand to prepare the HR material with the room temperature (RT) free carrier density less than 10^7 cm^{-3}, which is used as a limit density for the HR material. The intrinsic concentration at 300K is approximately 8×10^5 cm^{-3} in CdTe. The doping to such a low density is up to now technologically impossible in CdTe and a presence of any shallow (fully ionized at RT) uncompensated level results in the free

carrier density well above the demanded value. This argument results in a necessity to prepare the CdTe, where (i) shallow donors and acceptors compensate mutually ($N_D = N_A$) or (ii) deep defects compensate the relevant shallow levels. In this case the deep donors (acceptors) with density N_{DD} (N_{AD}) compensate the uncompensated shallow acceptors (donors), respectively. The Fermi level is pinned to the deep level, if the relations between densities $N_{DD} + N_D > N_A > N_D$ or $N_{AD} + N_A > N_D > N_A$ are fulfilled. It must be mentioned that the identification of deep defects (donor or acceptor) is difficult in samples where shallow defect density is unknown. We shall present the theoretical results assuming deep donor doping in this paper. The alternative model with deep acceptor is evident. Simulations of resistivity in dependence of the position of Fermi level were discussed for CdTe in Ref. [22] and for (CdZn)Te in Ref. [23].

The realistic description of defect structure in CdTe asks to include both extrinsic and native defects into the model. Contrary to the extrinsic defect density which is temperature and pressure independent, the native defect densities can be tuned by a proper annealing at defined thermodynamic conditions. The situation can be, moreover, complicated by an interaction between defects, which results in a formation of complexes. We shall neglect the formation of complexes first to simplify the theoretical description. The effect of complexes to the model will be discussed subsequently.

The native defects, which dominate in near stoichiometric samples CdTe are Cd interstitial (Cd_I, divalent donor) and Cd vacancy (V_{Cd}, divalent acceptor) [3,18]. The equilibrium densities of neutral native defects are given by reaction constants [24]

$$\left[Cd_I^X\right] = \frac{n_o\sqrt{T}P_{Cd}}{K}\exp\left[-\frac{1}{k_bT}\left(E(Cd_I) + U(Cd_I)^{vib}\right) + S(Cd_I)^{vib}\right], \tag{7}$$

$$\left[V_{Cd}^X\right] = \frac{n_oK}{\sqrt{T}P_{Cd}}\exp\left[-\frac{1}{k_bT}\left(E(V_{Cd}) + U(V_{Cd})^{vib}\right) + S(V_{Cd})^{vib}\right]. \tag{8}$$

$$\tag{9}$$

Relevant defect formation energy E, vibrational energy U^{vib} and entropy S^{vib} in Table I were obtained from the *ab initio* calculations and by fitting the high temperature transport data

[3].

$$K = k_b T^3 \left(\frac{m_{Cd} k_b}{2\pi\hbar^2} \right)^{3/2},$$

$n_o = 1.48 \times 10^{22}$ cm^{-3} is the number of unit cells per volume, k_b is the Boltzmann constant, and m_{Cd} is the mass of Cd atom. The label X is used for neutral defects overall.

The densities of multiply ionized defects are calculated for acceptors and donors

$$\left[X^{z-}\right] = \left[X^X\right] \frac{g_{X^{z-}}}{g_{X^X}} \exp\left(\frac{z\mu_F - E_a^1 - ... - E_a^z}{k_b T} \right), \tag{10}$$

$$\left[X^{z+}\right] = \left[X^X\right] \frac{g_{X^{z+}}}{g_{X^X}} \exp\left(\frac{E_d^1 + ... + E_d^z - z\mu_F}{k_b T} \right), \tag{11}$$

where E_a and E_d are the acceptor and donor one-electron ionization energies and $g_{X^{z-}}$, $g_{X^{z+}}$ and g_{X^X} are the degeneracy of the defects. The index z means the ionization degree. The list of experimentally determined ionization energies of native defects is given in Table II. The experimentally determined energy gap E_g according to [25] is used at all temperatures. The Fermi energy μ_F is obtained solving the electric neutrality condition

$$n + \left[V_{Cd}^-\right] + 2\left[V_{Cd}^{2-}\right] + N_A^- = p + \left[Cd_I^+\right] + 2\left[Cd_I^{2+}\right] + N_D^+ + N_{DD}^+. \tag{12}$$

All extrinsic defects (N_A, N_D, N_{DD}) are assumed monovalent here. Due to the complicated structure of the conduction band both Γ and L minima are taken into account [10].

The dynamic of native defects is controlled by the chemical self-diffusion described well by the chemical diffusion coefficient given by Eq. 6. It determines the minimum temperature for the fast diffusion of native point defects in bulk samples. At low T the diffusion is slow and only long-time annealing or thin samples must be used to reach the equilibrium.

TABLE II. The energy and entropy terms which fit the high temperature experimental data. The underlined parameters were optimized [3]. The others are from *ab initio* calculations [18,24]. Two energies for the Cd_I correspond to the two tetrahedral interstitial sites.

Defect	$E + U^{vib}$(eV)	$S(k_b)$
Cd_I	0.96; 1.29	<u>11.1</u>
V_{Cd}	<u>3.55</u>	<u>-5.6</u>

TABLE III. The ionization energy and degeneracy of Cd_I and V_{Cd}. Both defects are divalent. Two energies for Cd_I correspond to the two tetrahedral interstitial sites. The vacancy energies are referenced in the Table, other data are according to [18,26].

Defect	E^1(meV)	g_1	E^2(meV)	g_2
Cd_I	0; 210	2	170; 360	1
V_{Cd}	50 [27]	2	470 [28]	1/3

D. Results and discussion

Before the start of the analysis of doped samples, the correct description of undoped CdTe is necessary. The knowledge of equilibrium concentrations of defects at high temperature obtained from *in situ* galvanomagnetic measurements allowed us to establish the position of the theoretical stoichiometry line (the so called p-n line) in the form [3]

$$P^S = 8 \times 10^5 \exp(-1.76 \times 10^4/T) \text{ (atm)}. \tag{13}$$

Theoretically, the annealing at P^S should result in a fabrication of undoped HR material. In reality, however, a small deviation from ideal stoichiometric annealing conditions results in a strong increase of native defect density. The necessary precision of setting the Cd pressure at P^S during the experiment is practically unrealizable and deep defect doping is necessary to extend the interval of P_{Cd} in which HR samples can be prepared.

The deep donor level in the midgap with the thermal ionization energy 0.75 eV below the conduction band is used in most of our calculations. Such a level was determined in Vanadium doped CdTe [29] and our general model will be finally demonstrated on samples doped by this element.

The electric neutrality condition (12) is solved numerically within the loop of the P–T diagram and the effect of deep donor doping to the fabrication of HR material is studied. We show in Fig. 7 the results of the calculations of the RT carrier density in a deep defect doped CdTe sample annealed at 600°C and varying P_{Cd}. The left-hand side of the figure, P_{Cd} <0.002 atm, is dominated by holes, the right-hand side shows the density of electrons. The practical impossibility to prepare undoped high-resistivity CdTe is demonstrated here. The density decreases below 10^7 cm^{-3} and the HR requirements are fulfilled only in a very narrow interval around the ideal stoichiometry line. The situation is not changed also in case of low doping density $N_{DD} = 10^{14}$ cm^{-3}. The interval of allowed P_{Cd} broadens and the HR conditions are fulfilled more easily increasing N_{DD}. Concurrently, higher N_{DD} implicates the carrier trapping and recombination and therefore poor detector properties

of such samples [21] due to a high total defect density in the crystal. Thus the optimum conditions must be looked for to grow the HR material at the minimized doping density with P_{Cd} being allowed to spread within a realistically wide interval. In view of the presented results the optimum doping density to prepare the HR material by annealing at 600°C gives N_{DD} in the region $10^{15} - 10^{16}$ cm^{-3}. The plateau in the hole density at $p \approx 10^{11} - 10^{12}$ cm^{-3} is due to the pinning of the Fermi level to the Cd-vacancy 470 meV above the valence band.

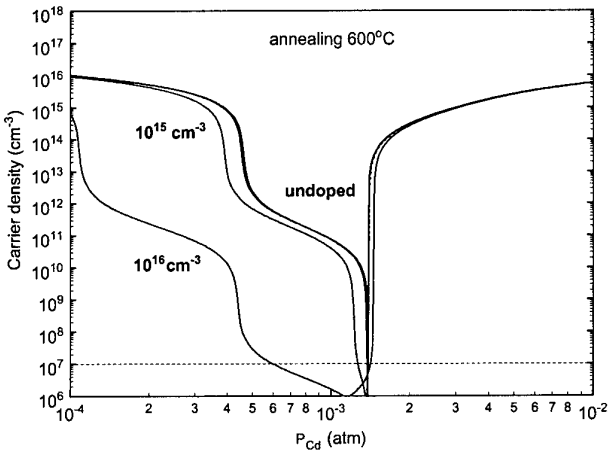

FIG. 7. Room temperature carrier density of deep defect doped sample annealed at 600°C. The black line corresponds to undoped CdTe, the green, blue and red lines correspond to 10^{14}, 10^{15}, and 10^{16} cm^{-3} doping, respectively. The HR limit density 10^{7} cm^{-3} is labeled as well.

The influence of annealing temperature to the discussed effects is demonstrated in Fig. 8, where annealing at 500°C was considered. Comparing to the case of 600°C, the HR material can be really reached with a lower deep doping density. Concluding from that the annealing of CdTe at lower T allows to reduce the necessary deep defect doping and the material with better quality can be obtained. Unfortunately, the annealing at low T extends the necessary time to reach the equilibrium and the long-time experiments must be performed.

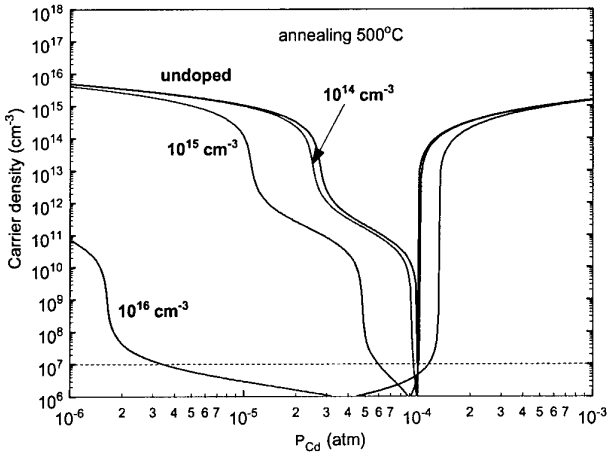

FIG. 8. Room temperature carrier density of deep defect doped sample annealed at 500°C. The black line corresponds to undoped CdTe, the green, blue and red lines correspond to 10^{14}, 10^{15}, and 10^{16} cm^{-3} doping, respectively.

The general impact of the annealing temperature on the fabrication of high resistive CdTe within the P-T diagram is demonstrated in Fig. 9.

The deep defect density results in the demands to the thermodynamic conditions, which must be set to obtain HR material. The HR regions for each N_{DD} are confined by the full and dash boundary lines being minimum and maximum P_{Cd}, respectively. The labels point to the corresponding N_{DD}. The upper limit of P_{Cd} for $N_{DD} \leq 10^{15}$ cm^{-3} merges in the stoichiometry line. In heavily doped samples ($N_{DD} = 10^{19}$ cm^{-3}) HR conditions are fulfilled overall in the stability region below maximum P_{Cd} labeled 10^{19}. We can deduce, that it is possible to prepare HR samples also with N_{DD} approaching to 10^{14} cm^{-3}, if anneling temperature $T < 450$°C is applied.

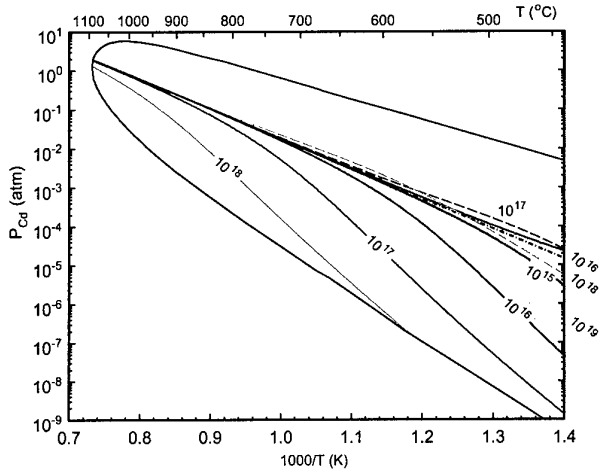

FIG. 9. Regions in the P–T diagram, where the high resistive deep defect doped CdTe can be obtained. The full (dash) lines mark respectively the minimum (maximum) P_{Cd}, which limit the HR region. Labels indicate corresponding doping density in cm^{-3}. For a plasticity, the HR region for doping 10^{16} cm^{-3} is highlighted. The ideal stoichiometry line for undoped CdTe (dash-dotted) is plotted as well. The minimum P_{Cd} for doping 10^{19} cm^{-3} results below the stability region.

The present technology does not allow to prepare CdTe without shallow extrinsic defects. Such defects influence the electric properties, especially the position of the p-n line, and subsequently the thermodynamic conditions for the fabrication of HR materials. We demonstrate the impact of shallow defects to the position of p-n line in Fig. 10, where its course for various shallow donor or acceptor doping (without deep defects) is plotted. The related RT carrier density is shown in Fig. 11. Besides the shift of HR region we observe also its narrowing due to the increasing native defect density far from P^S.

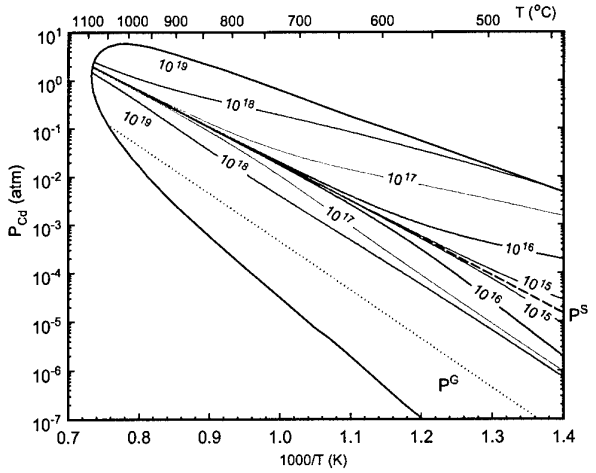

FIG. 10. The effect of extrinsic shallow defect doping to the position of the p-n line in P–T diagram. The labels mark the density of extrinsic defects for given p-n line. The donor doping shifts p-n line downward P^S, the acceptor doping upward P^S. The dash and dotted lines show the ideal stoichiometry line P^S and the line of congruent sublimation P^G, respectively.

The set of defects in CdTe should be completed by complexes, which are often mentioned in the literature. In our case a complex of deep donor with V_{Cd} should be taken into account. At the high temperature, at which the annealing is performed, the complexes are probably unstable and dissociate to the simple species. Their involvement is thus not needed in the high temperature calculations. During the cooling, when the sample passes through medium temperatures, where the complexes become stable and the short range diffusion is sufficiently fast to allow the complex formation, new related defect levels (possibly shallow) evolve in the gap. The complex formation can have two inevitable consequences for the HR samples. (i) The density of single deep donors decreases as they are lost by the complex formation. (ii) New complex levels act as new shallow acceptors or donors and must be included into the electric neutrality calculation (12). Consequently, the Fermi level could drop off the midgap and the resistivity can significantly decrease.

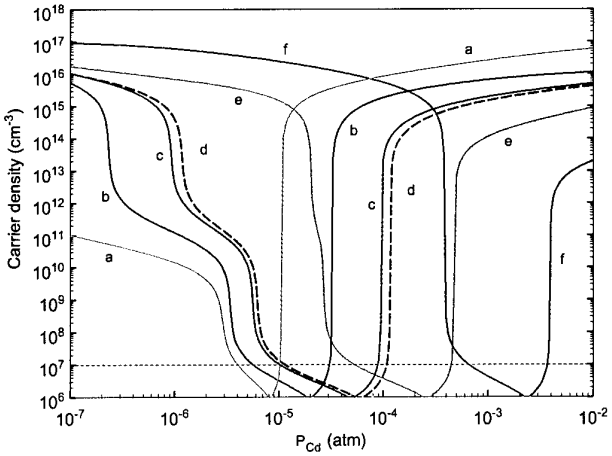

FIG. 11. Room temperature carrier density of sample annealed at 500°C for various shallow doping density at $N_{DD} = 5 \times 10^{15}$ cm^{-3}. The dash line plots the zero shallow doping, the labeled lines a, b, c correspond to 10^{17}, 10^{16}, 10^{15} cm^{-3} shallow donor doping, d, e, f to 10^{15}, 10^{16}, 10^{17} cm^{-3} shallow acceptor doping, respectively.

For a simple estimation within our model, we assume, that shallow acceptor complex X comes up via reaction of deep donor with V_{Cd} and moreover all V_{Cd} enter in the complex or recombine with Cd_I, i.e. $[X] = [V_{Cd}] - [Cd_I]$, and foreign shallow defects being neglected. Then the criteria for HR sample without complex $N_{DD} > 2([V_{Cd}] - [Cd_I]) > 0$ transform into $N_{DD} - [X] > z[X]$, where z is the valence of the complex. If $z = 1$, the situation is not influenced by the complex formation and the sample remains high resistive. If $z > 1$, the region for the fabrication of HR material in P-T diagram (Fig. 9) narrows and the deep defect density must be increased or annealing temperature decreased to fit the HR region well.

Vanadium is often used as a typical deep defect in CdTe. The position of its level formally identified to the V^{2+}/V^{3+} single donor in Cd site was found in the midgap with the thermal ionization energy 0.75 eV below the conduction band [29]. If such an interpretation is correct, two shallow donor levels of V must be compensated by native or foreign acceptors in Cd sites

to prepare HR V-doped material. In view of the previous discussion the compensation by foreign shallow acceptors is preferred. They compensate the material near the stoichiometry line where the tuning of the position of the Fermi level by the variation of P_{Cd} is the most effective. For the practical demonstration we show in Fig. 12 the resistivity of V-doped sample annealed at 500°C with ideally compensated shallow levels.

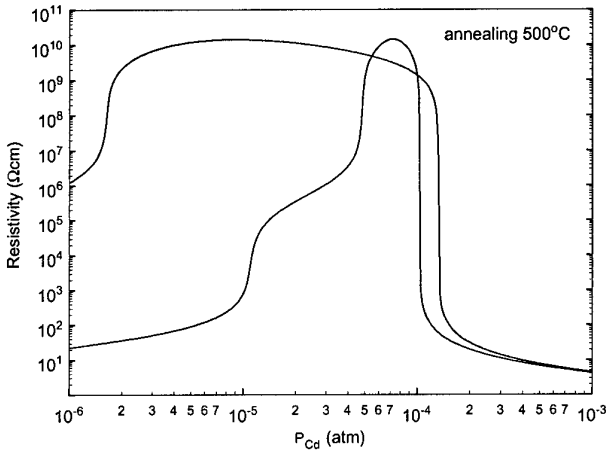

FIG. 12. The room temperature resistivity of V-doped sample with ideally compensated shallow levels annealed at 500°C as a function of annealing Cd pressure. The red and blue lines correspond to the V-doping densities 10^{16} and 10^{15} cm^{-3}, respectively.

E. Conclusion

Methods for fabrication of high resistivity detector-grade CdTe are discussed. Thermodynamic conditions at which an undoped material is stoichiometric are found based on high temperature *in situ* galvanomagnetic measurements, when two major native defects - the Cd vacancy and the Cd interstitial are applied in model calculations. It is demonstrated, that only a small deviation from stoichiometric conditions results in a strong generation of native defects and therefore in a crystal resitivity decrease. This makes the fabrication of a high resistivity undoped CdTe a problem, which is difficult to solve with the state-of-the-art

technological possibilities. Modelling of room temperature crystal resistivity in dependence of the concentration of a dopant with the energy level near the middle of the gap and thermodynamic conditions, from which the crystal is quenched to room temperature is performed. It is shown, that when increasing the deep defect density the range of optimal P_{Cd} at each annealing temperature broadens and the high resistivity can be reached more easily. The influence of shallow extrinsic defects and complexes of native defects with the deep dopant results in shifting and narrowing of the $P_{Cd}(T)$ range, where the high resistivity material can be obtained. The presented model can be generalized to any structure of defect levels in CdTe.

V. DEFECT INDUCED OPTICAL TRANSITIONS IN CDTE

While at high temperatures in CdTe native point defects play a dominant role in not intentionally doped crystals, room and low temperature optical and galvanomagnetic properties are often strongly influenced by residual impurities. The photoluminescence is a favorite method used for a study of defect structure. Systematic effort was devoted to find out the binding energy of shallow acceptors by low temperature photoluminescence (PL), PL excitation spectroscopy and magnetooptical analysis [30–32]. Doping experiments performed on high purity materials have shown, that all studied acceptors are related to substitutional impurities [30]. Contrary to a large amount of papers devoted to photoluminescence on CdTe and related compounds, optical absorption studies are rare. Infrared absorption (400-2000 cm^{-1}) in Cu doped CdTe was analyzed in [33], while combined photoluminescence and absorption measurements of the 1.1 eV deep band related to Te vacancies were performed in [34]. Irregularities in the structure of absorption edge in CdTe were explained in [35] by a phonon assisted direct excitonic absorption. The shape of the absorption spectra as well as the interpretation, which agrees qualitatively with our paper, was reported for ZnTe in [36]. In this paper we evaluate the absorption below the absorption edge of CdTe and $Cd_{1-x}Zn_xTe$. We use a model of totally charged classical acceptor impurity band, where the

Coulomb interaction is screened by mobile charges in partially filled level.

A. Experimental

CdTe and CdZnTe (with the Zn content ~4%) single crystals were fabricated in our laboratory by the Vertical Gradient Freeze method [17]. 6N purity starting elements were used in all growth runs. The Cd pressure at the maximum temperature during the growth was reached by adding of the corresponding amount of Cd in the ampoule. All crystals were very good quality single crystals filling about 90% of the crucible volume with no macroscopical defects (grain boundaries, twins), p-type with the room temperature concentration $\sim 10^{13}$ cm^{-3}. No intentional doping was applied. For our PL and optical absorption studies samples with thickness 1.5-3 mm were prepared by cutting, polishing and etching in Br-methanol solution.

The transmittance spectra (resolution 1 cm^{-1}) were measured by Fourier transform spectrometer IFS66/s (Bruker) and He flow cryostats VSK 4-300 (Leybold).

B. Theory

The structure of the absorption edge in semiconductors is generally determined by four effects which are responsible for the finite absorption constant α below the principal band-edge energy E_g. 1. The exciton absorption is observed below E_g forming free exciton with binding energy in CdTe 10.6 meV, and the donor and acceptor bound exciton at 13 meV and 16.8 meV, respectively. 2. The band edge is broadened due to the lattice disorder, which results in the exponential tail in the density of states and is manifested also in α. 3. The lattice defects initiate localized states in the gap. The absorption connected with the electron transfer into/from these levels allows to characterize them and to establish their ionization energies. 4. All transitions can be accompanied by the phonon assisted processes, at low temperature characterized by the emission of optical phonon at the energy

21.2 meV in CdTe. The effect results in the repeated characteristic structure accompanying the transitions in item 3.

The purpose of this paper is to explain the absorption 20 - 70 meV below E_g at low temperature (4-20K), where the remarkable details were found (see Fig. 13). In respect to the items 1.-4. above we can eliminate the excitonic effects, which are not observed at such energies. The exponential broadening of the absorption edge forms the background absorption in this region. The characteristic wavy shape is not, however, explained by this mechanism. Based on given remarks, we suggest that the mechanism in item 3 can be expected to describe the observed effect.

The single impurity↔band absorption constant is calculated by a standard way according to [37,38] in the form

$$\alpha_1(\hbar\omega) = \frac{16\,e^2\,P^2\,g}{3\,c\,\varepsilon_0\,n\,\hbar^2\omega}\left(\frac{\hbar^2}{2\,m^*\,a_B^2}\right)^{5/2}\frac{\sqrt{\hbar\omega - E_g + E_I}}{\left(\frac{\hbar^2}{2\,m^*\,a_B^2} + \hbar\omega - E_g + E_I\right)^4}, \tag{14}$$

where $P = 8.5 \times 10^{-8}$ eVcm is the momentum matrix element [39], n is refractive index, and e, c, ε_0, $\hbar$ are elemental constants. We shall show in the discussion that the absorption is connected with the acceptor–conduction band (CB) transitions, where the acceptors are charged due to compensating donors. In this case the acceptor degeneracy $g = 4$, E_I ($\equiv E_A$) and a_B are the acceptor binding energy and Bohr radius in the effective mass approximation and $m^* = 0.096m_0$ is the CB effective mass.

At the low temperature, when the free particle density can be neglected, the potential at the localized states is influenced by the Coulomb interaction with charge on other point defects. Consequently, E_A fluctuates around its ideal single-acceptor value and the impurity band (IB) with the density of states $G(E)$ is formed. The energy deviation of the respective acceptor is obtained in the form

$$\delta E_A(\mathbf{r}) = \frac{e}{4\pi\varepsilon_0\varepsilon_r}\Sigma_s\frac{Z_s}{|\mathbf{r} - \mathbf{r_s}|}, \tag{15}$$

where Z_s is the charge of the respective site. The total absorption constant α is obtained integrating

$$\alpha = \int_{E_g-\hbar\omega}^{\infty} \alpha_1(\hbar\omega + X - E_A)\, G(X)\, dX, \tag{16}$$

where $G(X)$ influences the start of the absorption which is smoothed comparing to the sharp increase in case of isolated acceptor level. The fitting of α to experimental data allows to estimate the shallow defect parameters. The magnitude of α determines the defect density and the start of the absorption gives the position of respective ionization level. The shape of the absorption edge is used for the examination of the relevant IB.

The impurity levels in CdTe are of very complicated structure forming both shallow and deep donor and acceptor states. The exact distribution of the levels is not known in our samples. In respect to this fact we use a minimal model here, which includes a set of shallow acceptors to describe the characteristics in the absorption, and one compensating donor level (does not matter if deep or shallow), placed sufficiently far above the valence band. While acceptors are assumed ionized (–), donors are partly neutral to fulfill the neutrality condition and the Fermi energy is placed near this level. The charge on donors (+) occupies preferentially the sites near acceptors and screens the Coulomb interaction. Its equilibrium distribution in finite temperature is obtained by Monte Carlo simulations [40–42].

The final states in CB are also disturbed by potential fluctuations. Their description is, however, much more complicated and runs to the necessity to solve the problem of localization in disordered systems. The solution of this task is out of the scope of this paper. We estimate such effect here using the well-known relation between binding, kinetic and potential energy E_b, $< T >$ and $< V >$, respectively, which reads in the hydrogen-like states $E_b =< T >= - < V > /2$. Relying to that we assume that the potential fluctuations of the CB edge manifest by one half in the transition energy and decrease twice the effective width of $G(E)$ in comparison to Eq. (15). On the contrary, the opposite action to G can be observed due to the unknown charged defects, both donors and acceptors, which increase the potential fluctuations and result in the increase of the width of G. The shape of the absorption edge can give an information about G, which can be thus used for the characterization of the samples with respect to their purity and make visible by the

indirect way the charged defects, which are not observed in other experimental methods. In our calculations we neglect first these effects assuming flat CB and include only the acceptor levels, which are observed in the absorption. The above mentioned corrections are subsequently discussed to become the more realistic model.

C. Results and discussion

The first task, which is to be solved is the decision about the type of the point defects which are responsible for the sub-gap transitions. As it is seen in Fig. 13, the absorption can be good approximated by the square root of energy in agreement with the numerator in Eq. (14). The denominator must have only weak influence. Such demand is easy fulfilled in case of acceptors for which $\hbar^2/(2\,m^*\,a_B^2) \sim 0.3$ eV for hydrogen-like acceptor is significantly greater than the energy interval of our interest. The opposite situation is met in case of transitions from valence band to donors, for which the factor above is significantly suppressed and α would have to pass maximum within the monitored interval. Another argument can be based on experimental findings [43], which report acceptor levels close to our observations. No donor level was reported in this region.

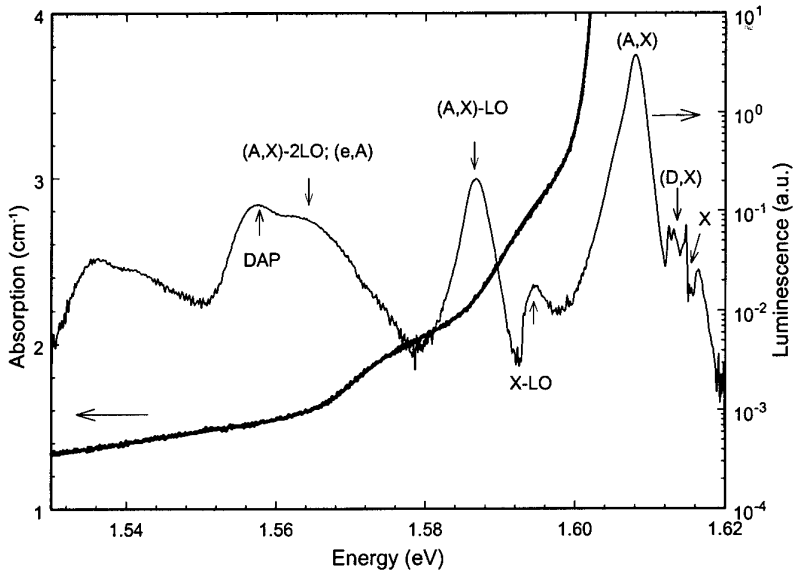

FIG. 13. Absorption and luminescence spectra of (CdZn)Te at 4.8K. The theoretical α is not resolved from experiment in this scale.

We present results of the fit of α on two our samples measured at 4.2 K. A very good agreement of theoretical fit with experimental absorption together with luminescence of sample $Cd_{0.96}Zn_{0.04}Te$ is presented in Fig. 13, for which $E_g = 1.625$ eV was established. We see the characteristic advancement of α near 1.57 eV, which is greatly fitted within presented model. The position of level $E_{A1} = 58.6$ meV agrees well with $E_{As} = 58 \pm 2$ meV and $E_{Sb} = 61 \pm 2$ meV [43]. The interpretation is also supported by the position of the donor-acceptor peak DAP in the luminescence, which is shifted to lower energy by the donor binding energy. The acceptor density at this level $N_{A1} = 2.8 \times 10^{14}$ cm^{-3} was calculated according to (14), (16), where the Bohr radius $a_{B1} = 10.5$Å was used [43].

The similar motif is repeated once more at higher energy 1.59 eV. We tried to describe this part by a new acceptor level with $E_{A2} = 38.2$ meV. Such level is not reported in the literature and its Bohr radius a_{B2} is thus not known. We connected a_{B2} with a_{B1} by the relation $a_{B2} = a_{B1}\sqrt{E_{A1}/E_{A2}}$, which yields $a_{B2} = 13.0$Å and resulting acceptor density

$N_{A2} = 3.2 \times 10^{14}$ cm^{-3}.

In the luminescence spectrum the standard free exciton (X), donor- (D,X), acceptor-bound excitons (A,X) and their phonon replicas are observed. A broad luminescence band at 1.55-1.58eV includes the DAP peak, the second phonon replica of the (A,X) and the peak corresponding to a transition from acceptor to the conduction band (e,A). Due to the fact, that these contributions to the luminescence band are not well resolved, determination of the energy level of the acceptor from the luminescence spectrum is difficult.

The detailed analysis of the results of the Monte-Carlo simulations on this sample is shown in Fig. 14, where the theoretical α, background absorption and the density of states G of the impurity bands is presented. We fit the background α by a linear and exponential functions, which fit properly peripheral parts of the investigated interval. The course of G of both levels is the same due to the same character of Coulomb interaction in our classical approach with the line width of FWHM=5.6 meV. The best fit was obtained with the compensating donor density $N_D = 9 \times 10^{14}$ cm^{-3}, whose variations influence slightly the shape of G.

The excellent fit was obtained within our very simple model of two shallow acceptors and one compensating donor. If the additional charges are included to the model, the IB broadens and the start of the absorption is smoothed. The influence of charged levels to α is demonstrated in Fig. 15, where new fully charged donor and acceptor levels with the same density were supplemented in the model calculations and the compensation of the sample was increased. The finding implies that the sample is pure without substantial concentration of other invisible charged defects. The situation could be complicated by the warping of the conduction band discussed in the Theory. If G is narrowed twice, the best fit is obtained with the invisible charge density $\sim 4 \times 10^{15}$ cm^{-3}. The careful study of CB in disordered systems is thus desirable.

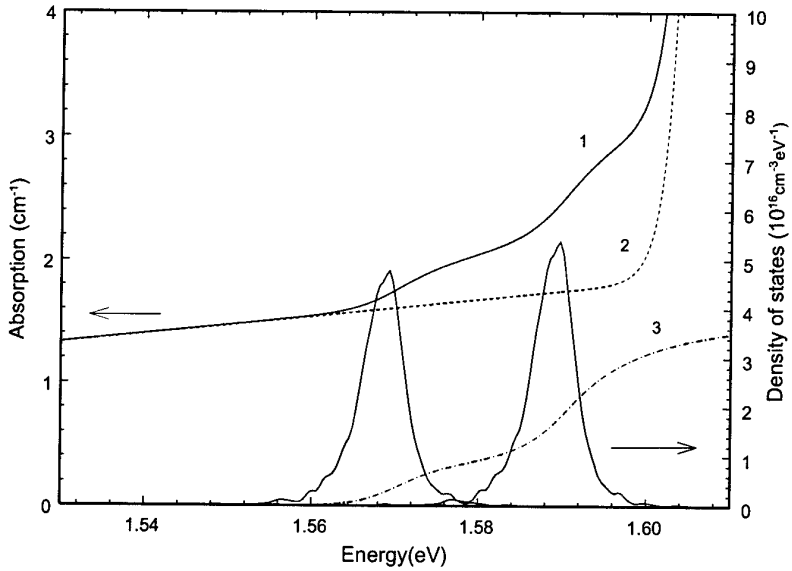

FIG. 14. Theoretical absorption of the (CdZn)Te sample (full line - 1), background absorption (dash - 2) and the absorption connected with acceptor-conduction band transition (dash-dotted - 3). The line 1 is the sum of lines 2 and 3. The peaks show the impurity bands density of states calculated by Monte-Carlo simulations on a cubic cell containing 4000 acceptors.

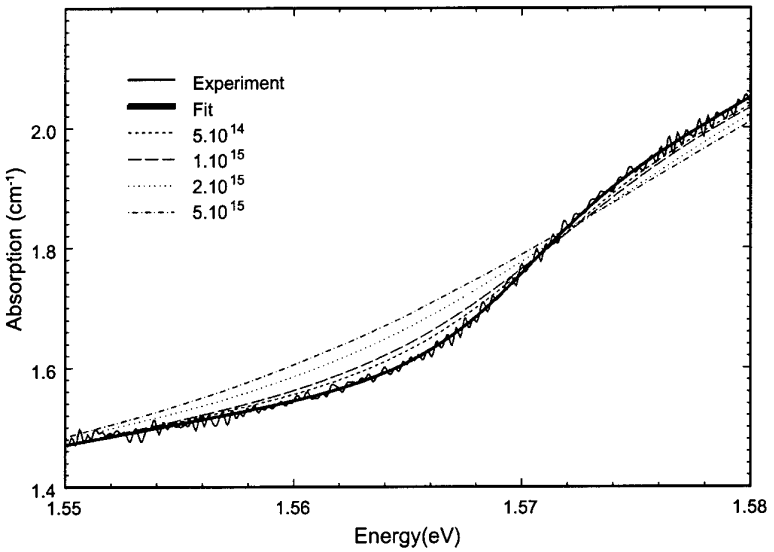

FIG. 15. The influence of the background doping to the shape of the absorption. The legend indicates the concentration of the additional donor N_D and acceptor N_A charged levels ($N_D = N_A$).

The interpretation of the second level E_{A2} is, however, not clear and alternative descriptions could be also valid in this case. The corresponding donor-acceptor peak is not observed in the luminescence and the ionization energy difference $E_{A1} - E_{A2} = 20.4$ meV is close to the optical phonon energy 21.2 meV. This finding points to a possibility to interpret this effect as a phonon assisted transition from the acceptor E_{A1}. Other plausible explanation could be accepted connecting the effect with the complicated structure of the band edge, which is responsible for the strong increase of α above 1.60 eV.

The results of the measurements and the fit of α on sample CdTe are plotted in Fig. 16 ($E_g = 1.605$ eV). The typical character of the absorption edge is also evident at 1.55 eV and the fit produces $E_{A1} = 59.0$ meV, again in good relation with DAP. The level density results $N_{A1} = 1.4 \times 10^{14}$ cm^{-3} in this case and the density of states FWHM=2.8 meV. Other acceptor level corresponding to the absorption edge near 1.57 eV is not well pronounced and cannot be fit within our model. As in the previous sample its position is again about

20 meV above E_{A1}, which supports the interpretation of this part by the mechanism of the phonon assisted absorption from the level E_{A1}.

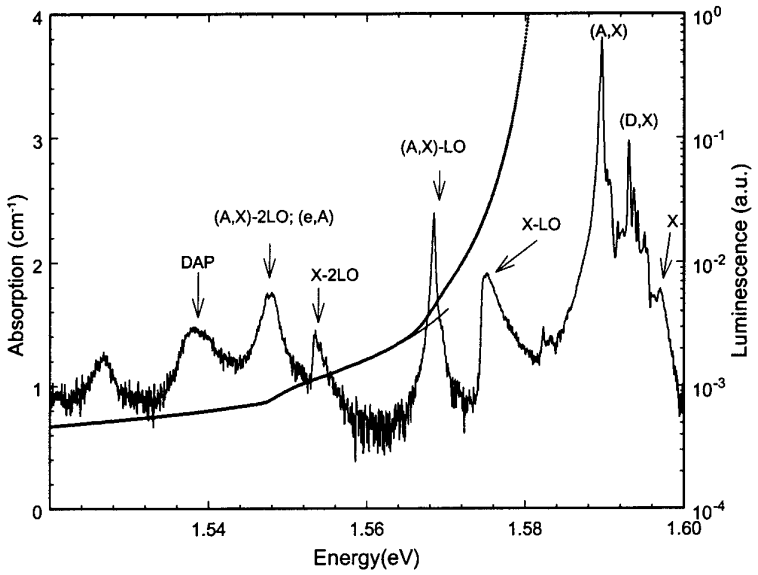

FIG. 16. Absorption and luminescence spectra of CdTe at 4.8K. The theoretical α deviates from experiment at 1.565 eV due to the complicated course of the absorption edge, which is not included in the model.

Comparing shape of the fundamental absorption edge in both samples, we observe the start of strong increase of α_f at similar energies relatively to E_g. In CdTe the fundamental absorption starts at about 20 meV lower energy relatively to E_g and corrupts partly the shape of α in the region of defect induced absorption. A seeming contradiction between FWHM of G, which implies a higher purity of the CdTe sample and the opposite result obtained from the shape of the absorption edge could be explained by a higher concentration of neutral defects in CdTe sample. Neutral defects do not manifest in the Coulomb broadening of G, they can, however, influence the band edge. The width of the impurity band enables to estimate the total concentration of charged impurities in the sample including deep defects, which are difficult to be observed by other analytical methods. The concentration of charged

defects in both samples is much lower than it could be deduced from the 6N purity starting elements. This result concludes, that foreign impurities are mostly neutral or form neutral complexes in our samples.

VI. REFRACTION INDEX OF CDTE: SPECTRAL AND TEMPERATURE DEPENDENCE

CdTe has considerable application in radiation detectors and other optoelectronics devices and is used as substrate for epitaxial growth, e.g. of HgCdTe layers for infrared detectors fabrication. Therefore, properties of CdTe have been investigated intensively. Many papers (e.g. [35,44–48]) reported on a spectral dependence of refractive index at room temperature (RT), a lot of works dealt with optical parameters above the gap energy at RT as well. Temperature dependence of the energy gap E_g has been investigated by various methods ([49] and references therein). Temperature dependence of the spectral position of a higher critical point E_1 was measured by Ksendzov et al [50]. Optical parameters above the energy gap were investigated at elevated temperatures (from RT to 727 K) by Kim and Sivananthan [51]. To our knowledge, no systematic study of temperature dependence of refractive index has been published.

The data reported in this paper were obtained by measurement of interference oscillations in transmittance for 20 temperatures between 10 K and 295 K. We tried to describe both the spectral and temperature dependence of the refractive index in the transparency range by simple empirical relations.

The sample used in our study was nominally undoped, high resistivity bulk CdTe. It was ground and polished to the thickness 54.6 μm, as determined by the surfometer SF 200 (Planer Products Ltd.). The transmittance spectra (resolution 1 cm^{-1}, 0.12meV) were measured using Fourier transform spectrometer IFS66/s (Bruker) and helium flow cryostats VSK 4-300 (Leybold). The divergence of the beam was decreased by a diaphragm down to 4^o. At temperature 10K, 430 interference maxima were recognized in the investigated

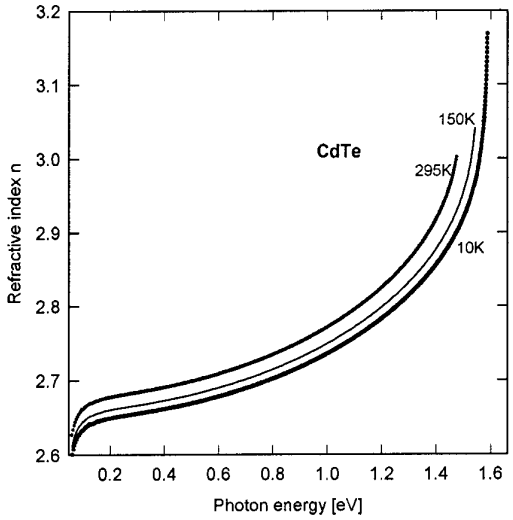

FIG. 17. Spectra of refractive index for temperatures 10K, 150K and 295K.

spectral range, while 377 maxima were observed at 295K due to a narrower spectral range of the sample transparency. The transmittance spectra near the absorption edge had been treated by a baseline procedure before the positions of the interference maxima were established. Each maximum was fitted by a cosine – like function to determine its position more accurately. Indices of refraction were calculated by well known formula for a position of interference maxima. The obtained spectra for three temperatures are shown in Fig. 17.

We compared our experimental results at RT with some of published relations. The differences reach several hundredths in the spectral region near the absorption edge, see Fig. 18a,b. Marple [35], Wei et al. [47] and Peiris et al. [48] used Sellmeier's formula for dispersion caused by one oscillator. The respective relations were obtained by fitting of the experimental values in various spectral ranges: Marple [35] 0.5 - 1.4 eV by method of minimum deviation at dispersion by the prism; Wei et al [47] 0.75 - 1.5 eV from ellipsometric data; Peiris et al. [48] 1.2-1.45 eV from oscillation of reflectivity on a MBE epitaxial layer and by a prism coupler technique at fixed wavelength 852.3 nm.

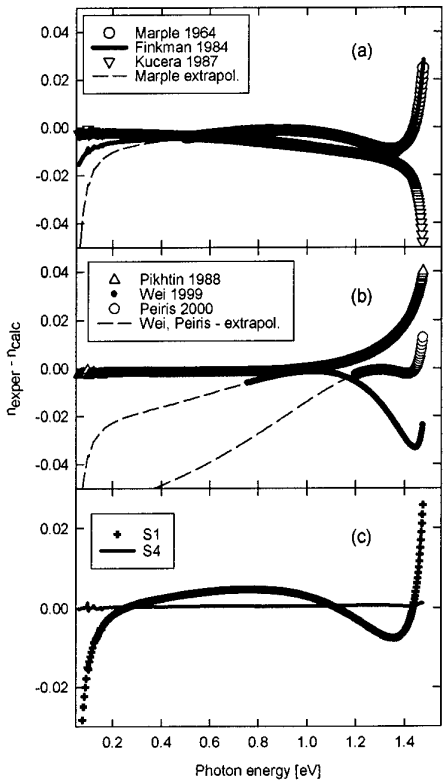

FIG. 18. (a),(b) Differences between our experimental data and values calculated from published empirical relations. (c) Crosses represent residuals in fitting procedure of our data at 295K to Sellmeier's formula (1-oscillator model). Solid line shows differences between the experimental data and calculation using Eqs. (17-22).

Finkman et al [44] supplied Sellmeier's formula by a term describing a decrease of the index at low photon energies due to phonons. Pikhtin and Yaskov [46] and Kucera [45] used in their fitting equations terms derived by the Kramers - Kronig transformation in a model of rectangular spectrum of imaginary part of dielectric function to take into account the band character of the energy spectrum.

The results of fitting of our experimental results by Sellmeier's formula can be seen in Fig. 18c for RT. A better agreement with experiment can be obtained by increasing the

number of the oscillators. It has been shown that model taking 4 oscillators into account (hereafter model S4) describes the spectra quite well. There is a lot of parameters in the model, some of them are interdependent in fitting procedures. We tried various assumptions concerning both the temperature dependence of oscillators energies and their strengths. Below we present relations obtained from a model (S4), where the oscillators strengths were assumed to be constant, excepting the strength of the "exciton" oscillator. Furthermore, the spectrally independent term, the energy and strength of the phonon oscillator could be fixed as well. After this simplification the form with 20 parameters was fit by the least square method to the experimental data

$$n^2(\omega) = a + \sum_{i=1}^{4} \frac{g_i}{E_i^2 - (\hbar\omega)^2}, \tag{17}$$

where $a = 3.153$, the term $i = 1$ denotes the contribution of optical transitions near band gap

$$E_1(T) = 1.5976 - \frac{6.09 \times 10^{-4} T^2}{T + 255}, \text{ [eV]} \tag{18}$$

$$g_1(T) = \left(0.0369 - \frac{9.26 \times 10^{-5} T^2}{T + 22.4}\right)\left(1 - \frac{0.0946}{1 + \exp(20 - \frac{555}{T})}\right), \text{ [eV}^2\text{]} \tag{19}$$

terms with i=2 and i=3 approximate an effect of all higher transitions

$$E_2(T) = 1.7102 - \frac{5.04 \times 10^{-4} T^2}{T + 208}, \text{ [eV]} \qquad g_2 = 0.3454\,\text{eV}^2, \tag{20}$$

$$E_3(T) = 3.2668 - \frac{2.794 \times 10^{-4} T^2}{T + 112.5}, \text{ [eV]} \qquad g_3 = 39.966\,\text{eV}^2, \tag{21}$$

and term $i = 4$ represents lattice vibrations

$$E_4 = 0.018\,\text{eV} \qquad g_4 = 9.02 \times 10^{-4}\,\text{eV}^2. \tag{22}$$

The precision of the fitted parameters is given with respect to their influence to the least square sum. It is surprising that this simplified model describes the experimental data so well with a maximum deviation near the absorption edge (about 20 meV below E_g) $\Delta n = \pm 0.002$. The error of n due to an uncertainty of the thickness of the sample is estimated to $\pm 0.5\%$.

The rise of the index with increasing temperature is caused by a decrease of the transition energies in a qualitative agreement with published dependence of gap energy [49] and energy of higher critical points [50,51]. The shifts of our parameters E_2 and E_3 are weaker than the reported shifts of the critical points.

Temperature dependence of E_1 is slightly different from the exciton energy (determined from the luminescence spectra) as shown in Fig. 19a. We let the parameter g_1 free during the fitting procedure to obtain a good agreement with experimental data. The non-monotonic temperature dependence with a well pronounced step near T=30K shown in Fig. 19b was approximated by a Fermi-Dirac-like term in Eq. (19). Irregularities near 30K are observed in the absorption as well. Spectral position of the absorption edge defined by the absorption coefficient 500 cm^{-1} is shown in Fig. 19a. These effects are caused by a temperature dependence of state population near the band edges due to irradiation of the sample in the spectrometer. We have measured the position of the absorption edge at extremely low intensity, which resulted in a shift of the edge down by 2 meV at 10K, see dashed line in Fig. 19a. We suppose that this correction could modify the fitted g_1 by removing the Fermi-Dirac-like term in (19). The exact verification of such model is, however, very difficult in our experimental setup because of noise in the interference oscillations at low radiation intensity.

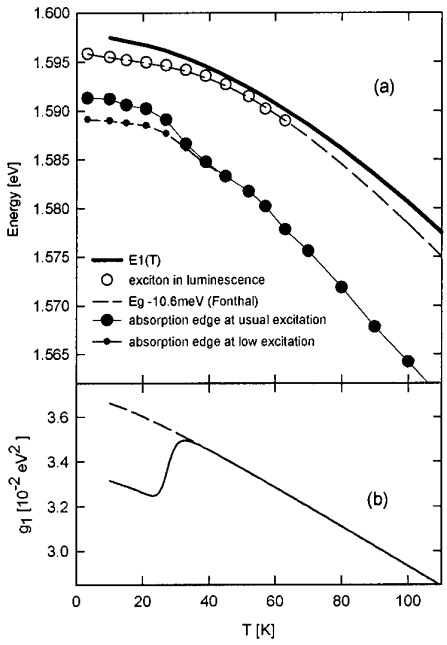

FIG. 19. (a) Parameter $E_1(T)$ compared with: exciton energy as determined from luminescence of our sample; with the relation $E_g(T)$ given by [49]; with the absorption edge defined by the value 500 cm^{-1} determined from measurement at usual intensity of radiation in the spectrometer (big circles) and at intensity 1000× lower (small circles). (b) Temperature dependence of the parameter g_1 as given by Eq. (19) (solid line) and g_1 expressed by the first bracket (without Fermi-Dirac term) in Eq.(19) (dashed).

The temperature dependences of the refractive index are shown in Fig. 20 together with the curves calculated from equations (17)-(22) for several wavelengths. The experimental values of refractive index at these wavelengths were determined by an interpolation between the nearest interference maxima.

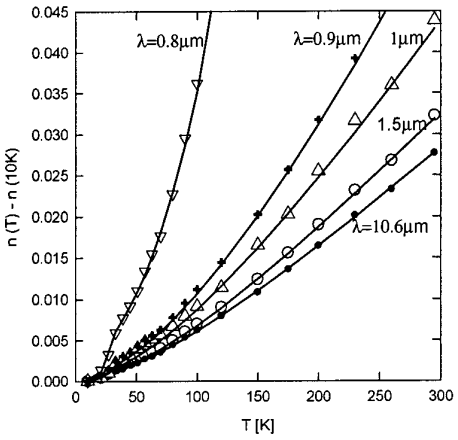

FIG. 20. Temperature dependence of refractive index for indicated wavelengths. Solid lines are calculated by Eqs. (17)-(22).

We can summarize that simple empirical relation can be used, approximating spectral and temperature dependence of the refractive index of CdTe with a good accuracy with maximum deviation $\Delta n = \pm 0.002$ near the absorption edge. This form can be used in practical applications and as a check in formula for a formulation of more realistic model complying with the band structure of CdTe.

REFERENCES

[1] R. F. Brebrick, Ching-Hua Su and Pok-Kai Liao, in Semiconductors and Semimetals (Ed. By R.K. Willard son and A.C, Beer) Vol. 19, p.171 Academic Press, New York (1983)

[2] J. P. Gaspard, C. Bergman, C. Bichara, R. Bellissent, P. Chieux and J. Goffart, J. Non-Crystalline Solids 97-98, 1283 (1987)

[3] J. Franc, P. Höschl, R. Grill, L. Turjanska, E. Belas, and P. Moravec, J. Electron. Mater. 6, 595 (2001)

[4] V. Glazov, S. Chizhevskaya, and N. Glagoleva, Liquid Semiconductors (Plenum Press, New York, 1969)

[5] L. Shcherbak, J. Crystal Growth 197, 397 (1999)

[6] Yu. V. Rud, K. V. Sanin, Sov. Phys.-Semicond. 6, 764 (1972)

[7] V. V. Godlevsky, J. J. Derby and J. R. Chelikowski, Phys. Rev. Lett. 81, 4959 (1998)

[8] M. Muhlberg, R. Rudolph, M. Laasch, and E. Treser, J. Crystal Growth 128, 571 (1993)

[9] J. Franc, R. Grill, P. Hlidek, E. Belas, L. Turjanska, I. Turkevych, A. L. Toth, P. Moravec and H. Siffer, Semicond. Sci. Technol. 16, 514 (2001)

[10] J. Franc, R. Grill, L. Turjanska, P. Hoschl, E. Belas, and P. Moravec, J. Appl. Phys. 89, 786 (2001)

[11] J. Franc, P. Hlidek, P. Sitter, E. Belas, A. L. Toth, L. Turjanska, and P. Höschl, Physica B 273, 883 (1999)

[12] C. Z. Van Doorn, Rev.Sci.Instr. 32, 755 (1961)

[13] P. Rudolph, in Recent Development of Bulk Crystal Growth (Ed. Milssiki), Research Signpost 1998 S. Mahajan, S. Mc. Dewitt and D. J. Johnson, p. 132

[14] H. N. G. Wadley, B. W. Choi, J. Cryst. Growth 172, 323 (1997)

[15] M. U. Ahmed, E. D. Jones, in EMIS Datareviews Series No. 10 Part B4.2 , Ed. P. Capper, INSPEC London 1987, p.466

[16] K. Zanio, J. Appl. Phys. 41, 1935 (1970)

[17] P. Höschl, Yu.M. Ivanov, E. Belas, J. Franc, R. Grill, P. Hlídek, P. Moravec, M. Zvára, H. Sitter, and A.L Toth, J. Crystal Growth 184/185, 1039 (1998)

[18] M. A. Berding, Phys. Rev. B60, 8943 (1999)

[19] Y. Eisen, A. Shor, J. Crystal Growth 184/185, 1302 (1998)

[20] P. Rudolph, S. Kawasaki, S. Yamashita, S. Yamamoto, Y. Usuki, Y. Konagaya, S. Matada, T. Fukuda, J. Crystal Growth 161, 28 (1996)

[21] L. Chibani, M. Hage-Ali, P. Siffert, J. Crystal Growth 161, 153 (1996)

[22] M. Fiederle, C. Eiche, M. Salk, R. Schwarz, K. W. Benz, W. Stadler, D. M. Hofmann, and B. K. Meyer, J. Appl. Phys. 84, 6689 (1998)

[23] A. Zumbiehl, P. Fougeres, M. Hage-Ali, J. M. Koerbel, P. Siffert, A. Zerrai, K. Cherkaoui, G. Marrakchi, and G. Bremond, J.Crystal Growth 197, 670 (1999)

[24] M. A. Berding , M. van Schilfgaarde, and A. Sher, Phys. Rev. B50 1519, (1994)

[25] D. Nobel, Philips Res. Rep. 14, 361 (1959)

[26] M. A. Berding, private communication.

[27] M. R. Lorenz, B. Segall, Phys. Lett. 7, 18 (1963)

[28] P. Emanuelsson, P. Omling, B. K. Meyer, M. Wienecke and M. Schenk, Phys. Rev. B47 15578 (1993)

[29] A. Zerrai, G. Marrakchi, and G. Bremond, J. Appl. Phys. 87, 4293 (2000)

[30] E. Molva, J. L. Pautrat, K. Saminaydar, G. Milchberg, N. Magneau, Phys. Rev. B30, 3354 (1984)

[31] W. Ossau, T. A. Kuhn, R. N. Bicknell-Tassius, J. Crystal Growth 101, 135 (1990)

[32] M. Stadler, D. M. Hofmann, H. C. Alt, T. Muschik, B. K. Meyer, E. Weigel, G. Müller-Vogt, M. Salk, E. Rupp, K. W. Benz, Phys. Rev. B51, 10619 (1995)

[33] J. Bajaj, S. H. Shin, P. R. Newman, J. E. Hoffman, M. G. Stafelbroek, J. Vac. Sci. Technol. A4, 2051 (1986)

[34] Ch. Barnett Davis, D. A. Allred, A. Reyes-Mena, J. Gonzáles Hernandéz, O. Gonzáles, B. C. Hess, W. P. Allred, Phys. Rev. B47, 13363 (1993)

[35] D. T. F. Marple, Phys. Rev. 150, 728 (1966)

[36] D. T. F. Marple and M. Aven, Proceedings of the Conference on II-VI Semiconducting Compounds, (Providence, September 1967) p. 315

[37] J. Callaway, *Quantum Theory of the Solid State* Academic Press, New York and London, 1974, p. 524

[38] V. Čápek, K. Zimmerman, Č. Koňák, M. Popova, and P. Polívka, phys. stat. sol. (b) 56, 739 (1973)

[39] M. H.Weiler, *Semiconductors and Semimetals Vol. 16*, ed R. K. Willardson and A. C. Beer Academic Press, New York, 1981, p. 119

[40] N. Metropolis, A. W. Rosenbluth, M. N. Rosenbluth, A. H. Teller, and E. Teller, J. Chem. Phys. 21, 1087 (1953)

[41] R. Grill, J. Phys.: Condens. Matter 7, 3565 (1995)

[42] F. A. Reboredo, Phys. Rev. B51, 5089 (1995)

[43] M. Soltani, M. Certier, R. Evrard, E. Kartheuser, J. Appl. Phys. 78, 5626 (1995)

[44] E. Finkman, S. E. Schacham, J. Appl. Phys. 56, 2896 (1984)

[45] Z. Kucera, Phys. Stat. Sol. (a) 100, 659 (1987)

[46] A. N. Pikhtin, A. D. Yaskov, Sov. Phys. Semicond. 22, 613 (1988)

[47] K. Wei, F. H. Pollak, J. L. Freeouf, D. Shvydka, A. D. Compaan, J. Appl. Phys. 85, 7418 (1999)

[48] F. C. Peiris, S. Lee, U. Bindley, J. K. Furdyna, J. Electron. Mater. 29, 798 (2000)

[49] G. Fonthal, L. Tirado-Mejía, J. I. Marin-Hurtado, H. Ariza-Calderon, J. G. Mendoza-Alvarez, J. Phys. Chem. Solids 61, 579 (2000)

[50] A. Ksendzov, F. H. Pollak, O. K. Wu, Solid State Commun. 70, 693 (1989)

[51] C. C. Kim, S. Sivanathan, J. Electron. Mater. 26, 561 (1997)